

Transition from two-dimensional to three-dimensional behavior in the self-assembly of magnetorheological fluids confined in thin slits

Ramin Haghgoie and Patrick S. Doyle*

Department of Chemical Engineering, Massachusetts Institute of Technology, Cambridge, Massachusetts 02139, USA

(Received 11 January 2007; published 28 June 2007)

We study the effects of extreme confinement on the self assembly of the colloids found in magnetorheological (MR) fluids using Brownian dynamics simulations. The MR fluid is confined in a thin slit with a uniform external magnetic field directed normal to the slit. We find a crossover in the behavior of the system from two dimensions to three dimensions as the slit thickness is increased. A simple model is presented to describe this crossover as a function of the slit thickness and volume fraction of the MR fluid. The model is able to predict the salient features of the structure formation that has been observed in these systems. Furthermore, the model predicts the approximate time scales for structure formation under a variety of conditions. We present a quantitative analysis of the effect of volume fraction on the behavior of the system. Additionally, we show quantitatively how energy barriers to structure formation play a crucial role in determining the steady state structure of these systems. Our analysis explains the discrepancies between previous experimental and theoretical work on the self-assembly of MR fluids confined in thin slits.

DOI: [10.1103/PhysRevE.75.061406](https://doi.org/10.1103/PhysRevE.75.061406)

PACS number(s): 82.70.Dd, 68.03.Hj, 75.40.Mg, 61.46.Bc

I. INTRODUCTION

The confined self-assembly of induced dipoles such as the kind found in magnetorheological (MR) fluids has been of great interest for many years from both a fundamental science standpoint and from a practical application standpoint [1–4]. The confinement of MR fluids can cause drastic changes in the nature of the structures that form under the application of an external magnetic field [2,5]. Recently, the self-assembled structures formed by MR fluids under the application of an external magnetic field have been used as structural components in microfluidic devices to perform size-dependent separations of DNA molecules [3,4]. In these devices, a low volume fraction MR fluid is self-assembled in a slitlike microchannel by the application of a uniform external magnetic field directed normal to the thin slit. The self-assembled structure formed by the MR fluid in this geometry resembles an array of columnlike clusters spanning the height of the channel. The spacing between these columns (or the pore size in the channel) is an important parameter for characterizing the efficacy of the DNA separation.

Columns can form in thin-slit channels when the volume fraction of MR colloids is less than about 0.1 and the external magnetic field is strong enough to overcome the Brownian motion of the colloids [1,2,6,7]. There has been much research done to measure and model how the spacing between the column structures in thin slits depends upon the thickness of the slit. The experimental investigations have been performed in slits with thicknesses ranging from ~ 10 to 1000 's of colloid diameters [1,2,5–7]. The theoretical investigations into this system have generally been performed at infinite external field strength (or zero temperature) [6,8,9]. All of the experiments and theoretical studies performed on this system have concluded that there is a power-law dependence on the spacing between columns as a func-

tion of the thickness of the slit [1,2,5,6,8,9]. However, there has been much disagreement about the exact value of the power law. A survey of the literature can convince one that it is generally agreed that the power law in thin slits with a thickness of ~ 10 to 100 's of colloid diameters is ~ 0.4 and as the slit thickness is increased to several 1000 's of colloid diameters the power-law transitions to ~ 0.6 [1,2,6,8]. All of the above results are generally applicable as long as the external magnetic field is large enough to overcome Brownian motion. However, as the magnitude of the external magnetic field approaches infinity, there is theoretical evidence that there should be in fact only a single power law dictating the spacing between columns as a function of the slit thickness [9].

It is well known that as the external magnetic field is slowly increased from zero to a large value, bulk field responsive fluids such as MR fluids undergo several structural transitions [7,10–12]. The first transition is from a gas of Brownian colloids to randomly distributed chains of colloids aligned in the field direction. This aggregation into chains is known as head-to-tail aggregation. As the field is further increased, the chains of colloids begin to aggregate laterally in order to form clusters of zipped chains. This secondary aggregation is known as zippering. Likewise, in confined MR fluid self-assembly the same transitions can occur as the external field magnitude is increased. These transitions are illustrated in Fig. 1 where we show a schematic of the evolution of the MR fluid structure from a randomly dispersed state (left) to the lowest energy state (right) in two different slit-thicknesses. In the top of Fig. 1 the lowest energy structure on the right consists of chains spanning the height of the thin slit and therefore only head-to-tail aggregation is necessary to form these structures. In the bottom of Fig. 1 the system must undergo both head-to-tail aggregation and the zippering transition. However, because of the confinement in a thin slit, the energy barriers associated with the zippering of chains of MR colloids can be large, thus preventing the system from reaching the lowest energy state. We will show

*Electronic address: pdoyle@mit.edu

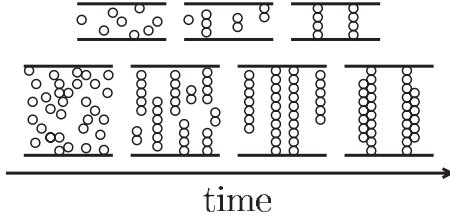


FIG. 1. Top: Schematic of the self-assembly of an MR fluid confined in a thin slit with a thickness equal to four colloid diameters. At time zero the MR fluid is a gaslike Brownian suspension and as the external field is slowly ramped the colloids aggregate head-to-tail in order to form chains spanning the height of the thin slit. Bottom: Schematic of the self-assembly of an MR fluid confined in a thin slit with a thickness equal to ten colloid diameters. At time zero the MR fluid is a gas of Brownian colloids and as the external field is slowly ramped the colloids first aggregate head-to-tail in order to form chains and then undergo a secondary zippering transition in order to reach the lowest energy state. There can be significant energy barriers to the zippering transition.

that one needs to take into account not only the lowest energy state of the thin-slit system but also the energy barriers associated with achieving that state in order to fully understand the self-assembly of MR fluids confined in thin slits.

The characteristic length scales in microfluidic devices are ever-shrinking and therefore it is likely that the thickness of the channels used for DNA separations will continue to shrink down to the fundamental limit of a single MR colloid diameter. In the extreme case where the thickness of the channel is equivalent to a single colloid diameter, the MR colloids will self-assemble in truly two-dimensional (2D) channels. As of yet, the self-assembly of dilute MR fluids in such extreme confinement has not been studied. Some work has been done to study the self-assembly of concentrated MR fluids (>0.2 volume fraction) under this extreme confinement but the structures that form at such high concentrations are not columnlike [13]. Some of the infinite field theoretical models mentioned previously can be extended down into the range where the slit thickness is less than ten colloid diameters but, as we will show, these models do not tell the whole story of the self-assembly in thin slits.

In this work we use Brownian dynamics (BD) simulations to study the self-assembly of dilute MR fluids under confinement in thin slits. We are interested in studying the phase space that is practical for the microfluidic DNA separation devices mentioned previously, namely, volume fractions <0.1 and external fields that are sufficiently large to cause structure formation but small enough that they can be experimentally realized. We note that there is a crossover from truly 2D behavior to the 3D behavior observed in the experimental systems mentioned above. We explain the mechanism of the crossover in these systems and discuss the important factors in determining where the crossover occurs.

II. SIMULATION DETAILS

Under the application of a uniform external magnetic field, the colloids in an MR fluid acquire dipole moments

aligned with the external field. The dipole moments cause the colloids to experience anisotropic interactions governed by the energy

$$U_{ij}(r_{ij}, \theta_{ij}) = \frac{m^2 \mu_0}{4\pi} \left(\frac{1 - 3 \cos^2 \theta_{ij}}{r_{ij}^3} \right), \quad (1)$$

where U_{ij} is the energy of interaction between two identical, parallel, point dipoles with magnitude m . The parameter μ_0 is the magnetic permeability of free space, the distance r_{ij} is the magnitude of the vector connecting the centers of colloids i and j , and θ_{ij} is the angle between the vector \mathbf{r}_{ij} and the external field vector. This interaction energy neglects the effects of mutual induction which can be present in real MR fluids but it has been successfully used to quantitatively predict the self-assembly of MR fluids [14]. Furthermore, the point dipole approximation has been shown to be a good approximation for the magnetic behavior of MR colloids [15]. The magnitude of the induced dipole moment of an individual colloid is given by

$$m = \frac{\pi}{6} d^3 \chi H_0, \quad (2)$$

where χ is the effective magnetic susceptibility of an individual MR colloid, d is the diameter of the colloid, and H_0 is the magnitude of the external magnetic field. The dimensionless field strength characterizing the magnetic interaction between MR colloids is given as

$$\lambda \equiv - \frac{U(d, 0)}{k_B T} = \frac{\pi \mu_0 d^3 \chi^2 H_0^2}{72 k_B T} \quad (3)$$

the ratio of the maximum magnitude interaction energy to the thermal energy in the system [2]. When $\lambda \gg 1$ then the MR fluid will self-assemble into structures aligned with the external magnetic field. The dimensionless interaction energy between two MR colloids is thus written as

$$\tilde{U}_{ij}(\tilde{r}_{ij}, \theta_{ij}) = \frac{1}{2} \lambda \left(\frac{1 - 3 \cos^2 \theta_{ij}}{\tilde{r}_{ij}^3} \right), \quad (4)$$

where d (the diameter of the colloids) is the characteristic length scale in this system.

The equation of motion for the colloids was given by

$$d\mathbf{r}_i(t) \simeq \frac{1}{\zeta} \mathbf{F}_{D,i}(t) dt + \frac{1}{\zeta} \mathbf{F}_{B,i}(t) dt, \quad (5)$$

where the inertia of the colloids is neglected [16–18]. The term $\mathbf{F}_{D,i}$ represents all of the deterministic forces acting upon colloid i and ζ is the drag coefficient on a single colloid. The term $\mathbf{F}_{B,i}$ is a stochastic term which is used to model the Brownian force acting on the colloid due to collisions with the solvent molecules. Hydrodynamic interactions between the colloids were neglected for simplicity. The deterministic forces in this system were due solely to the magnetic interactions between the colloids and are defined as

$$\mathbf{F}_{D,i}(t) \equiv \sum_{j \neq i}^N -\nabla U_{ij}[r_{ij}(t), \theta_{ij}(t)], \quad (6)$$

where N is the number of colloids in the system. The stochastic term is defined as

$$\mathbf{F}_{B,i}(t) = \sqrt{2\zeta k_B T} \frac{d\mathbf{W}_i(t)}{dt}. \quad (7)$$

The parameter \mathbf{W}_i is a Wiener process with

$$\left\langle \frac{d\mathbf{W}_i(t)}{dt} \right\rangle = 0, \quad (8)$$

$$\left\langle \frac{d\mathbf{W}_i(t)}{dt} \frac{d\mathbf{W}_j(t')}{dt'} \right\rangle = \delta_{ij} \delta(t-t') \boldsymbol{\delta},$$

where δ_{ij} is the Kronecker delta, δ is the Dirac delta function, and $\boldsymbol{\delta}$ is the identity tensor.

The equation of motion was integrated forward in time using a simple Euler integration scheme. At the end of a time-step, hard sphere overlaps were treated by displacing overlapped colloids along the line connecting their centers until they are just contacting [19]. In this manner, we project out any unphysical moves that may occur during the course of a time step. This procedure was performed for all overlaps, between two colloids and between colloids and hard walls [17,18], and was iterated until all overlaps in the system were removed.

The boundary conditions of the simulations in this work were periodic in the x and y directions and hard walls in the z direction. The uniform external magnetic field was directed in the z direction (normal to the thin slit) causing the MR colloids to self-assemble into column structures spanning the height of the thin slit. Simulations were performed for the self-assembly of five different volume fractions of MR fluid ($\phi=0.01, 0.03, 0.04, 0.05,$ and 0.07) in thin slits ranging in dimensionless thickness from $\tilde{L}=1$ to 30. The simulations were done in boxes with dimensionless lengths of 60, 35, 35, 30, and 30 in the x and y directions for the volume fractions 0.01, 0.03, 0.04, 0.05, and 0.07, respectively. Therefore, the number of colloids in the simulations ranged from 69 to 3 610 depending upon \tilde{L} and ϕ .

A dimensionless time step of $\Delta\tilde{t}=10^{-4}$ was used with time made dimensionless as $\tilde{t}=t(k_B T)/(\zeta d^2)$, where $(\zeta d^2)/(k_B T)$ is the time necessary for an MR colloid to freely diffuse a distance equal to its diameter. A dimensionless cutoff for the dipole-dipole interaction of 20 was used along with a linked-list binning algorithm [20] where the bin sizes were slightly larger than the cutoff value. Therefore, only interactions between colloids separated by a distance less than the cutoff were considered. The simulations were started from a random configuration and the external magnetic field strength was ramped continuously from $\lambda=0$ to $\lambda=50$ over a dimensionless time of 100 after which it was held constant at $\lambda=50$. Ramping the external magnetic field over a longer time did not change the final properties measured in the simulations. We tracked the spacing between the columns (or clusters) formed by the MR colloids until it remained constant

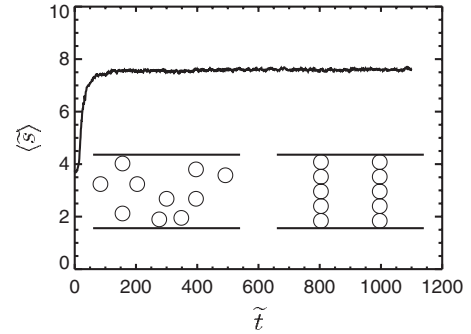


FIG. 2. The average dimensionless spacing between clusters $\langle \tilde{s} \rangle$ versus dimensionless time for a typical simulation ($\tilde{L}=5$) where the dimensionless external magnetic field is ramped from $\lambda=0$ to $\lambda=50$ over a dimensionless time of 100 and then held constant at 50 until the system reaches steady state. The inset on the left shows a typical random starting configuration and the inset on the right is an example of the final, steady-state structure.

for a dimensionless time of at least 100 before we began to collect statistics. All of the simulations were determined to be converged in system size, time step, and cutoff for the dipole-dipole interaction, and ramp time for the external magnetic field. For each set of conditions (ϕ and \tilde{L}), six separate trajectories were simulated (all from different starting configurations) in order to obtain a reasonable average for the physical properties of the structure and dynamics in these systems. An example of an equilibration curve for $\tilde{L}=5$ and $\phi=0.01$ is shown in Fig. 2. Schematics of the initial and final states of the system are shown as insets in Fig. 2.

The average spacing between clusters was calculated in the following manner as illustrated in Fig. 3. Starting with a snapshot of the system configuration (Fig. 3, left), the (\bar{x}, \bar{y}) position of the center of mass was calculated for each continuously connected cluster of MR colloids resulting in a 2D projection of the thin slit system in the x - y plane (Fig. 3, middle). MR colloids were considered to be connected if they were in hard-sphere contact. A Delaunay triangulation was performed on the 2D projection in order to determine the nearest neighbors of each cluster (Fig. 3, right). The average distance between clusters was then calculated as the average distance between nearest neighbor clusters.

III. TRANSITION FROM 2D TO 3D

As mentioned above, the previous work on the self-assembly of MR fluids in thin slits under the application of a

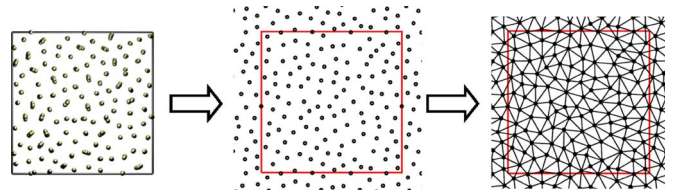


FIG. 3. (Color online) Left: Top view of the simulation box. Middle: 2D projection of the centers of mass of all the clusters in the simulation box. The red line represents the periodic boundaries of the simulation box. Right: Delaunay triangulation of the 2D projection showing the nearest neighbors of all of the clusters in the simulation box from which the average spacing can be calculated.

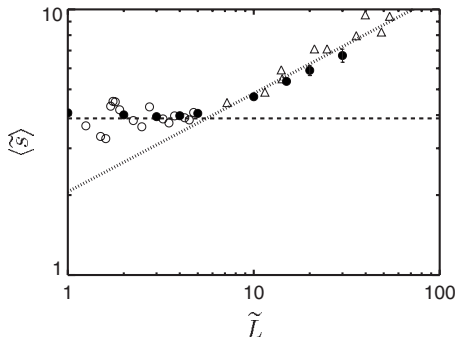


FIG. 4. Dimensionless spacing between clusters as a function of dimensionless slit thickness for $\phi=0.04$. The simulation data are shown as circles (closed circles are integer values of \tilde{L}). The simulations were performed at $\lambda=50$. The experimental data of Liu *et al.* [2] (performed at $\lambda=166$) are shown as open triangles. The dashed line is the spacing for a 2D system at the same ϕ given by Eq. (9) and the dotted line is the empirical power law given by Eq. (10) that Liu *et al.* fit to their experimental data.

uniform external magnetic field normal to the slit has all been done in slits with dimensionless thicknesses ranging from $\tilde{L} \sim 10$ to 1000 's. We are interested in probing the properties of self-assembled MR fluids under much tighter confinement ($\tilde{L}=1$ to 30) as there are many interesting properties of these systems that have not been observed in the previous work. In Fig. 4 we present our simulation results (circle symbols) for the average dimensionless spacing between clusters as a function of the dimensionless slit thickness for $\phi = 0.04$. We compare our simulation results to the experimental results of Liu *et al.* [2] (triangle symbols) for the same system. The dashed (horizontal) line in Fig. 4 represents the spacing between colloids at this volume fraction for a purely 2D system. This spacing is defined as [17]

$$\langle \tilde{s} \rangle_{2D} \equiv \sqrt{\frac{\pi}{2\phi_A\sqrt{3}}} = \sqrt{\frac{\pi}{3\phi\sqrt{3}}}, \quad (9)$$

where ϕ_A is the area fraction of colloids which, for a monolayer of colloids, is related to ϕ as $\phi_A = 1.5\phi$. The dotted (power-law) line in Fig. 4 is the empirical power law that Liu *et al.* found to best fit their data in the range $\tilde{L} \lesssim 200$ and is given by

$$\langle \tilde{s} \rangle = 2.058\tilde{L}^{0.37}. \quad (10)$$

The spacing in our simulations follows very closely the spacings from the experimental work of Liu *et al.* [2] for dimensionless slit thicknesses between 10 and 30. However, the two most interesting features of the data shown in Fig. 4 are the deviation from the empirical power law for slit thickness < 10 and the large oscillations in the spacing between clusters as a function of the slit thickness for extremely thin slits ($\tilde{L} \leq 5$). The deviation from the power law is expected intuitively but the details have not been previously explored. The large oscillations that occur in the dimensionless spacing for extremely thin slits are discussed elsewhere [21].

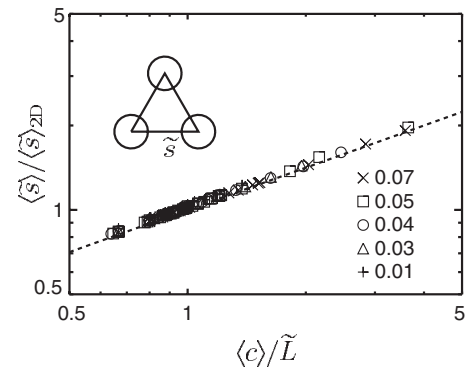


FIG. 5. Average spacing between clusters as a function of the average cluster size in the system. Data for five different volume fractions are presented. The dashed line is the prediction given by Eq. (13) and the inset is a schematic top-view of a triangular arrangement of clusters with circular cross sections.

In discussing the deviation from the power-law behavior, we are in essence discussing the transition from 3D to 2D behavior in these systems. For this, it will be useful to relate the cluster spacing to the average cluster size in the system. Using simple geometric arguments we can relate the average cluster size in the thin-slit system to the average cluster spacing as shown in Fig. 5. We define the average cluster size as $\langle c \rangle = N/N_c$, where N_c is the number of clusters in the system. If we assume that the clusters all have a dimensionless circular cross sectional area \tilde{A}_c and are arranged in a triangular lattice with dimensionless spacing \tilde{s} as shown in the inset of Fig. 5 then the area fraction of clusters is equal to the area fraction in a triangular lattice

$$\phi_A \equiv \frac{N_c \tilde{A}_c}{\tilde{A}} = \frac{\frac{1}{2} \tilde{A}_c}{\frac{\sqrt{3}}{4} \tilde{s}^2}, \quad (11)$$

where \tilde{A} is the dimensionless area of the x - y plane. Using the definition of the volume fraction

$$\phi \equiv \frac{N\pi}{6\tilde{A}\tilde{L}} \quad (12)$$

we can first substitute the definition for the average cluster size ($\langle c \rangle = N/N_c$) into Eq. (12) for N and then we can further substitute for the ratio N_c/\tilde{A} from Eq. (11). Making these two substitutions into Eq. (12) and rearranging we arrive at the relationship between the average spacing between clusters as a function of the average cluster size

$$\langle \tilde{s} \rangle = \sqrt{\frac{\pi}{3\phi\sqrt{3}} \frac{\langle c \rangle}{\tilde{L}}} \quad (13)$$

which is plotted as the dashed line in Fig. 5.

When $\tilde{L} = \langle c \rangle$ Eq. (13) reduces to Eq. (9), the value for the dimensionless spacing in the 2D system. This means that if the clusters are simply chains with a single colloid width spanning the height of the thin slit, the average spacing be-

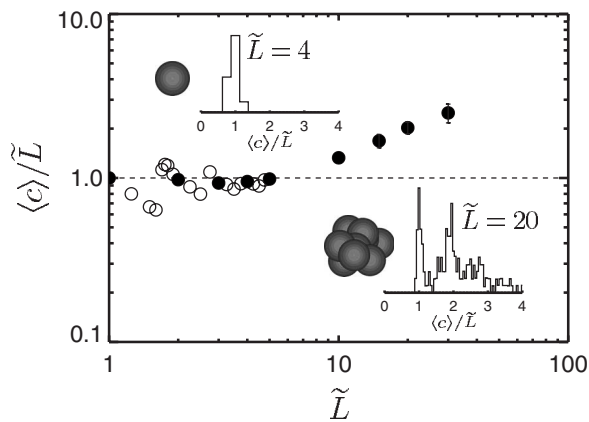


FIG. 6. Average cluster size as a function of dimensionless slit thickness for $\phi=0.04$. The solid circles represent integer values of the dimensionless slit thickness \tilde{L} . The horizontal dashed line represents the case where the clusters are single colloid width chains spanning the slit thickness. The top inset is a histogram of the distribution of cluster sizes in a thin slit with $\tilde{L}=4$ along with a top-view image of a characteristic cluster under these conditions. The bottom inset is a histogram of the distribution of cluster sizes in a thin slit with $\tilde{L}=20$ along with a top-view image of a characteristic cluster containing zipped chains.

tween those chains should be equal to $\langle \tilde{s} \rangle_{2D}$. We independently measured the average dimensionless spacing between clusters and the average cluster size in our simulations for all ϕ and \tilde{L} and plotted them in Fig. 5. The relationship between average spacing and the cluster size is very well predicted by Eq. (13). In our BD simulations we have access to the properties of the individual clusters (arrangement and number of colloids within a cluster) which are not easily accessible in experimental systems so we can relate changes in the average spacing between clusters to specific changes in the properties of the clusters themselves. In the experimental work, only general shape properties of the clusters have been used to explain the spacing behavior as a function of slit thickness [1,2]. The relationship between cluster properties and average spacing [Eq. (13)], will become important in later discussions of spacing as a function of slit thickness and volume fraction.

For instance, the crossover in the behavior of the dimensionless spacing from 2D to 3D as shown in Fig. 4 is directly related to the more complex clustering occurring as the slit thickness is increased. This point is illustrated in Fig. 6 where it is evident that the crossover in the spacing between clusters is directly correlated with the crossover from clusters which are single chains spanning the height of the thin slit ($\langle c \rangle / \tilde{L} = 1$) to clusters containing several “zipped” chains. Recall from the introduction that zipped chains are chains of MR colloids directed in the external field direction which have aggregated laterally to form larger clusters [12]. For a dimensionless slit thickness of 4 (Fig. 6, top inset) most of the clusters are chains containing 4 colloids spanning the height of the thin slit ($\langle c \rangle / \tilde{L} = 1$). For a dimensionless slit thickness of 20 (Fig. 6 bottom inset) there is a bimodal distribution of cluster types. There is a distinct peak at $\langle c \rangle / \tilde{L}$

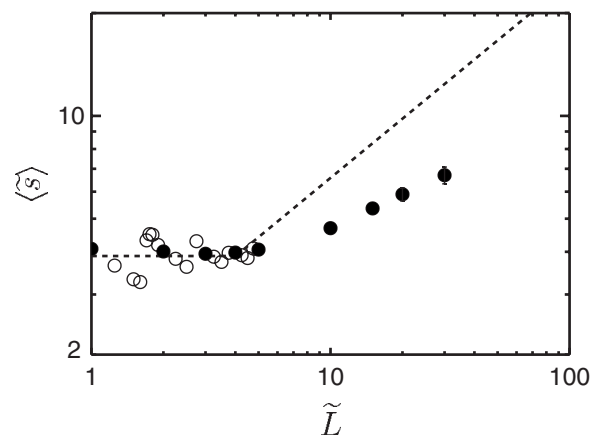


FIG. 7. Average dimensionless spacing as a function of dimensionless slit thickness. The dashed line is the spacing predicted by the Gross model [9]. The closed symbols represent integer values of \tilde{L} .

$= 1$ implying that a significant fraction of the clusters are single chains spanning the height of the thin slit while there is another, much broader, peak representing clusters consisting of several zipped chains. Again, in Fig. 6 oscillations occur in the average cluster size as a function of the slit thickness for $\tilde{L} \leq 5$ which are discussed elsewhere [21].

There have been several models created to describe both the spacing between clusters and the cluster sizes themselves as a function of the slit thickness in these systems [2,6,9]. The model developed by Grasselli *et al.* [6] assumes the clusters are ellipsoids spanning the height of the thin slit and containing enough colloids so that there is a distinct surface and bulk for each cluster. This assumption breaks down for thin slits, where $\tilde{L} \lesssim 30$ since the clusters under such confinement only contain a handful of colloids and are quite discrete in nature. Similarly the model developed by Liu *et al.* [2] assumes cylindrical clusters spanning the height of the thin slit and again containing distinct surface regions and bulk regions. Therefore this model also breaks down for $\tilde{L} \lesssim 30$ since it relies on a continuum description of the clusters. The model developed by Gross [9] considers discrete colloids arranged in clusters with either body-centered-tetragonal (bct) or face-centered-cubic (fcc) internal structures at infinite field strength.

The Gross model calculates the infinite-field lowest-energy configuration of the colloids in the system for each slit thickness. Using Eq. (13), the average cluster size predicted by the Gross model can be translated into an average spacing between clusters. The prediction for the average spacing as a function of slit thickness from the Gross model is shown in Fig. 7 dotted line along with our simulation results. The Gross model only makes predictions for integer values of \tilde{L} and therefore we will concentrate for now on those slit thicknesses (filled circles in Figs. 4, 6, and 7). For $\tilde{L} \leq 4$ the lowest energy state of the system as predicted by the Gross model consists of clusters with $\langle c \rangle = \tilde{L}$. Our simulation results match the predictions of the Gross model for the integer values of \tilde{L} in this range. However, for $\tilde{L} \geq 5$ there

are significant deviations between our simulation results (as well as experimental results [2] shown in Fig. 4) and the predictions by the Gross model for the lowest energy state. When we quench our simulations to zero temperature, we find that the energy in the system is higher than the energy for the configurations predicted by the Gross model. This implies that our simulations (and the experimental results [2]) are indeed in metastable states and do not reach the ground state configurations.

The discrepancy in power laws was noted by Gross who offered the following postulate for why experimental observations of spacing versus slit thickness do not match the predictions from his theoretical, infinite-field, model. Gross conjectured that for low volume fractions and high external field strengths the energy barriers for chain aggregation (zippering) may not be able to be overcome over laboratory time scales and therefore many of the experimental results for the thin-slit system were possibly trapped in states that do not correspond to the ground state at infinite external magnetic field [9]. This comment has the potential to explain the behavior that has been observed experimentally [2] and that we have observed in our simulations but it has not been elaborated upon in satisfying detail in the literature. We will now show that the presence of energy barriers can dictate many of the properties of self-assembled MR fluids in thin slits where $\tilde{L} \leq 30$.

A. Energy barriers to chain aggregation

Two rigid chains of MR colloids aligned parallel to one another interact with an energy $\tilde{U}_c(\tilde{r})$ that has the general form shown in Fig. 8(a) [14]. The energy curve consists of two parts [Fig. 8(a), inset]. The attractive energy well on the left can exist if the chains have a net attraction once they have zipped and the approach energy on the right exists for all parallel chains as they approach one another laterally. For large \tilde{r} all parallel chains have a repulsive interaction and as they approach each other that repulsion increases [the maximum in Fig. 8(a)]. If the chains are “uniformly parallel,” meaning that they are of the same length and are not shifted vertically with respect to one another, then their interaction is always repulsive and there is no “zipped” energy well. However, if the chains are shifted with respect to one another or are of different lengths then there can be a “zipped” energy well in their interaction energy. In fact, if the two chains are small enough such that they can undergo head-to-tail aggregation as illustrated in Fig. 8(b), then there exists a path for their aggregation with little or no energy barrier at all. Therefore, head-to-tail aggregation between individual MR colloids or short chains can readily occur in the thin-slit system as long as it is geometrically feasible. The vertical line on the left hand side of the energy curve in Fig. 8(a) represents the hard-sphere excluded volume potential when two chains are completely aggregated. Increasing the dimensionless external magnetic field strength λ will cause the maximum and minimum in Fig. 8(a) to increase in magnitude. The exact form of $\tilde{U}_c(\tilde{r})$ can be calculated for any two rigid chains by simply summing the dipole-dipole interactions between all of the colloids in the two chains.

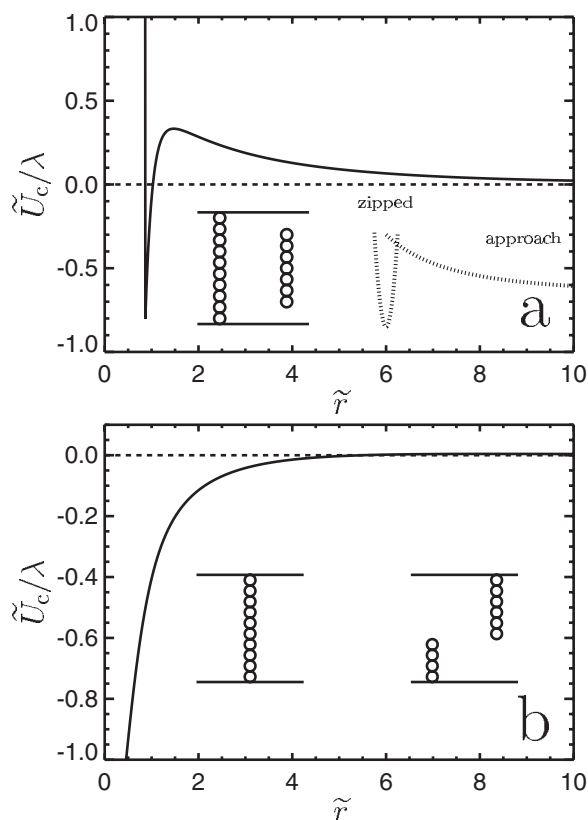


FIG. 8. (a) The general form of the interaction energy between two chains of MR colloids (in arbitrary units) as a function of their separation distance. The right inset illustrates the two parts of the energy curve, the approach energy and the zipped energy. The left inset illustrates the configuration of chains undergoing zippering. (b) The form of the interaction energy between two short chains which are able to undergo head-to-tail aggregation. The inset illustrates the configuration of the two short chains before (right) and after (left) head-to-tail aggregation.

The discussion of the energy barriers is relevant to the results presented in Fig. 7. When $\tilde{L} \leq 4$ the lowest energy state of the system as predicted by the Gross model is single colloid width chains spanning the height of the thin slit. As illustrated in Fig. 8(b), the head-to-tail aggregation necessary to form the single chains does not involve any significant energy barrier and therefore the system is not kinetically limited from reaching the lowest energy state. For $\tilde{L} \geq 5$ the lowest energy state of the system as predicted by the Gross model consists of clusters containing zipped chains. However, in Fig. 8(a) we illustrate that the zippering of chains involves energy barriers which have to be overcome in order to form the larger clusters predicted by the Gross model. As mentioned previously, this idea has been postulated in the literature [9,14] but a more quantitative analysis will be presented here. We have developed a simple model to quantify the energy barriers to zippering under the extreme confinement studied in this work. Our model attempts to calculate the potential energy barriers to aggregation for various global constraints (N , \tilde{L} , and ϕ) in order to determine when the thin-slit system is kinetically limited from reaching the

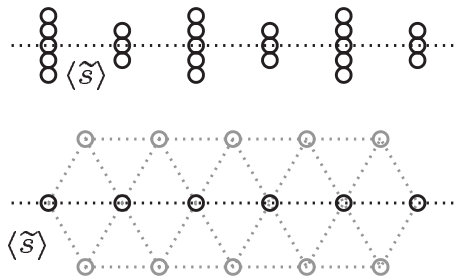


FIG. 9. Top: A side view of the one-dimensional periodic line where the neighbor pairs of clusters are all identical. Bottom: Top-down view of a hexagonal arrangement of chains in a thin slit, where the lattice spacing is $\langle \tilde{s} \rangle$. The model considers the highlighted lattice vector (considered to be a one-dimensional periodic line).

lowest-energy state as predicted by the Gross model. Our model differs from previous attempts to model the energy barriers to zipping [14] in that we include the effects of volume fraction which physically accounts for additional net attraction forces between chains, due to the surrounding chains, which must be added to the simple picture presented in Fig. 8.

B. Model

In the real thin-slit system, we have a fixed number of colloids N in a box with a fixed height \tilde{L} and a fixed volume fraction ϕ such that the ratio N/ϕ is also fixed. Recall that $N = N_c \langle c \rangle$ so the previous fixed ratio can be written as $N_c \langle c \rangle / \phi$. Therefore, once N , \tilde{L} , and ϕ have been determined, we can instead fix \tilde{L} , N_c , and $\langle c \rangle / \phi$. The ratio $\langle c \rangle / (\tilde{L} \phi)$ can be determined and $\langle \tilde{s} \rangle$ can therefore be considered fixed for given values of N_c , \tilde{L} , and $\langle c \rangle / \phi$. We find that fixing N_c , $\langle \tilde{s} \rangle$, and \tilde{L} (given N , \tilde{L} , and ϕ) leads to more useful conclusions from our model.

Therefore, consider a periodic one dimensional system of N_c rigid chains aligned with the external field and interacting with dimensionless energy $\tilde{U}_c(\tilde{r})$ (made dimensionless with $k_B T$). For simplicity, the chains only interact with their two nearest neighbors along the line and the entire system is under the global constraints mentioned above such that

$$\sum_i n_i \equiv N_c \quad (14)$$

and

$$\sum_i n_i \tilde{r}_i \equiv N_c \langle \tilde{s} \rangle, \quad (15)$$

where n_i is the number of pairs of neighboring chains with separation \tilde{r}_i . The motivation for this model is illustrated by the dark circles in the bottom of Fig. 9, where we observe that the top-down view of the thin-slit system looks similar to a hexagonal lattice in the ideal case with spacing between clusters given by $\langle \tilde{s} \rangle$. The line of dark circles in the bottom of Fig. 9 represents a lattice vector, and in this simplified picture can be considered the one-dimensional periodic system

we are modeling (without the effects of the neighboring lattice vectors). This model is an oversimplified version of the true structure of the system and is therefore only an approximation. However, the results derived from such a model provide significant insight into the behavior of the thin-slit system.

The Boltzmann weighted probability of having a set of separations $\mathbf{n} = \{n_0, n_1, \dots\}$ in our model is

$$\omega(\mathbf{n}) = \frac{N_c!}{n_0! n_1! \dots} e^{-\tilde{U}_c^{\text{tot}}}, \quad (16)$$

where \tilde{U}_c^{tot} is defined as

$$\tilde{U}_c^{\text{tot}} \equiv \sum_i n_i \tilde{U}_c(\tilde{r}_i). \quad (17)$$

We want to find the set of separations that maximize the probability given in Eq. (16) under the constraints given by Eqs. (14) and (15). Using Lagrange multipliers we write the maximization function as

$$\frac{\partial}{\partial n_i} \left[\ln \left(\frac{N_c!}{\prod_i n_i!} \right) - \sum_i n_i \tilde{U}_c(\tilde{r}_i) - \alpha \sum_i n_i - \beta \sum_i n_i \tilde{r}_i \right] = 0. \quad (18)$$

Solving Eq. (18) using Stirling's approximation for the first term on the LHS we are left with the result

$$n_i^* = C e^{-[\tilde{U}_c(\tilde{r}_i) + \beta \tilde{r}_i]}, \quad (19)$$

where the constant C comes from the first Lagrange multiplier (α) and is found by applying the first constraint [Eq. (14)]. Substituting in for the constant term we find

$$n_i^* = \frac{N_c e^{-[\tilde{U}_c(\tilde{r}_i) + \beta \tilde{r}_i]}}{\sum_i e^{-[\tilde{U}_c(\tilde{r}_i) + \beta \tilde{r}_i]}}. \quad (20)$$

Applying the second constraint and substituting Eq. (13) for $\langle \tilde{s} \rangle$ we can solve for the Lagrange multiplier β with

$$\frac{\int \tilde{r} e^{-[\tilde{U}_c(\tilde{r}) + \beta \tilde{r}]} d\tilde{r}}{\int e^{-[\tilde{U}_c(\tilde{r}) + \beta \tilde{r}]} d\tilde{r}} = \sqrt{\frac{\pi \langle c \rangle}{3 \phi \sqrt{3} \tilde{L}}}, \quad (21)$$

where we have replaced the sums over i with integrals over the separation distance \tilde{r} . Equation (21) can be solved numerically for β once we specify $\tilde{U}_c(\tilde{r})$, ϕ , $\langle c \rangle$, and \tilde{L} . More importantly, in this model the probability density that two chains will be separated by a distance \tilde{r} is given by

$$P(\tilde{r}) = \frac{e^{-[\tilde{U}_c(\tilde{r}) + \beta \tilde{r}]}}{\int e^{-[\tilde{U}_c(\tilde{r}) + \beta \tilde{r}]} d\tilde{r}} \quad (22)$$

meaning that the dimensionless potential energy between two neighboring chains is equivalent to $\tilde{U}_c(\tilde{r}) + \beta \tilde{r}$.

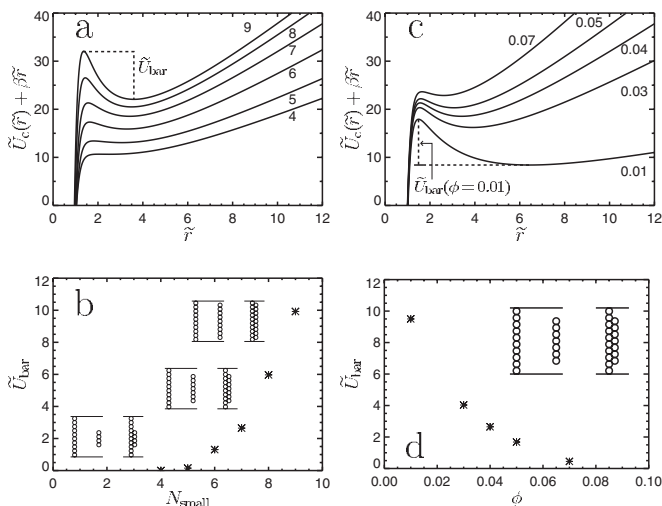


FIG. 10. (a) The dimensionless potential energy between neighboring chains of length 10 and N_{small} for six different small chain lengths ($N_{\text{small}}=9, 8, 7, 6, 5,$ and 4 from top to bottom) at a dimensionless field strength of $\lambda=50$ in a dimensionless slit thickness of $\tilde{L}=10$. The potential energy barrier to aggregation is shown for $N_{\text{small}}=9$. (b) The dimensionless energy barrier to aggregation as a function of N_{small} at a volume fraction of 0.04 and a dimensionless field strength of 50 . Insets are illustrations of the systems presented in this figure before aggregation (left) and after aggregation (right) for $N_{\text{small}}=9, 7,$ and 4 from top to bottom. (c) The dimensionless potential energy between neighboring chains of length 10 and 7 for five different volume fractions ($0.07, 0.05, 0.04, 0.03,$ and 0.01 from top to bottom) at a dimensionless field strength of $\lambda=50$ in a dimensionless slit thickness of $\tilde{L}=10$. The potential energy barrier to aggregation is shown for $\phi=0.01$. (d) The dimensionless energy barrier to aggregation as a function of volume fraction for a chain of length 10 and a chain of length 7 . Inset is an illustration of the system presented in this figure before aggregation (left) and after aggregation (right).

Again, the general form of the interaction between two rigid chains undergoing a zipper aggregation is shown in Fig. 8(a). Recall that the specific form of $\tilde{U}_c(\tilde{r})$ depends upon the two types of chains and λ . If we take the part of the function $\tilde{U}_c(\tilde{r})$ that lies to the right of the maximum, we can calculate β for a specific system given ϕ , $\langle c \rangle$, and \tilde{L} using Eq. (21). Furthermore, we can then use β to calculate the potential energy between two neighboring chains [$\tilde{U}_c(\tilde{r}) + \beta\tilde{r}$]. An example of the potential energy between a rigid chain of 10 MR colloids and rigid chains of different lengths (N_{small}) in a thin slit with $\tilde{L}=10$ (such that the large chain is strictly confined by the top and bottom of the thin slit) is shown in Fig. 10(a). The volume fraction of the MR fluid in this case was taken to be 0.04 and the dimensionless field strength was $\lambda=50$. The two interacting chains were assumed to be aligned in the vertical direction along the centerline of the thin slit but shifted such that they can undergo a zipper aggregation as illustrated in Fig. 10(b) (insets). The curves in Fig. 10(a) illustrate the effect that β has upon the interaction between two chains in this model. Physically, β is the parameter that takes into account the presence of

other chains in the system. For instance, if the two test chains in Fig. 10(a) move far away from one another, the energy $\tilde{U}_c(\tilde{r}) + \beta\tilde{r}$ actually increases because they are moving closer to the other chains in the system (i.e., they increase the total energy in the system). Therefore, the value of β will depend upon the volume fraction in the system and the types of chains for which the interaction energy is being calculated.

The idea of a volume fraction dependence upon the interaction between chains has been speculated before by Mohebi *et al.* [14]. In their work, the authors define a separation distance between chains called an escape distance below which two chains will zipper and above which the two chains will repel one another. They allude to the fact that as the volume fraction is increased, chains will be in closer proximity to one another and therefore more likely to enter the escape distance of their neighboring chains. However, this effect has not been quantified in the literature and here we present a quantitative analysis of the volume fraction dependence.

The curves in Fig. 10(a) show a local energy minimum near a dimensionless separation of ~ 4 which increases in magnitude as N_{small} is increased. In order for two chains to zipper (have a dimensionless separation distance < 1) they must pass through the transition state in their interaction energy [the maxima near $\tilde{r} \sim 1.5$ in Fig. 10(a)] before reaching the aggregated state. The difference between the local energy minimum and the transition state energy is the energy barrier to aggregation \tilde{U}_{bar} . In Fig. 10(a) the energy of the transition state as a function of N_{small} is increasing faster than the local energy minimum and therefore the energy barrier to aggregation increases with N_{small} . When $\tilde{U}_{\text{bar}} \sim 1$ two chains can zipper relatively easily by diffusion. In Fig. 10(b) we see that for a small chain length $N_{\text{small}} \leq 6$ the dimensionless energy barrier to aggregation is ≤ 1 implying that the two chains can easily undergo the zipper aggregation. This means that for a given \tilde{L} , ϕ , and λ there can be a critical small chain length (N_{small}^*) such that for any chain smaller than N_{small}^* it is energetically likely that it will zipper with a chain of length $N_{\text{big}} = \tilde{L}$ that is exactly confined between the parallel planes of the thin-slit.

In Fig. 10(c) we show the dimensionless potential energy between a chain of length 10 and a chain of length 7 at several different volume fractions in a dimensionless slit thickness of 10 with $\lambda=50$. This illustrates the effect that the volume fraction has upon the interaction between neighboring chains since increasing the volume fraction causes the energy barrier to aggregation to decrease. By increasing the volume fraction, the chains are forced to be closer together. This closer proximity means that they have less freedom to diffuse away from their neighbors and therefore β will be larger. The larger value of β causes the local minima in Fig. 10(c) to increase much faster than the local maximum (transition state energy) and therefore the energy barrier to aggregation is reduced with increased volume fraction. As a result, the ability for two chains to undergo a zipper aggregation depends heavily upon the volume fraction in the system as shown in Fig. 10(d), where the energy barrier shrinks significantly as ϕ is increased.

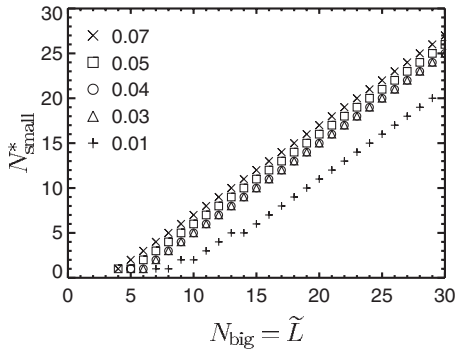


FIG. 11. Critical small-chain length as a function of dimensionless slit-thickness for five different volume fractions at a dimensionless field strength of $\lambda=50$.

We are interested in knowing when zippering aggregation barriers are small as a function of the slit thickness and therefore, we applied our model to the following problem. For a fixed slit thickness, we calculated the energy barriers for the zippering of one rigid chain which spanned the height of the thin slit ($N_{\text{big}}=\tilde{L}$) and another rigid chain with a length $1 \leq N_{\text{small}} \leq \tilde{L}-1$. The vertical position of the small chain was determined as

$$\begin{aligned} \text{if } N_{\text{big}} - N_{\text{small}} \text{ is even: } \tilde{z}_{\text{small}} &= \frac{\tilde{L}}{2} - 0.5, \\ \text{if } N_{\text{big}} - N_{\text{small}} \text{ is odd: } \tilde{z}_{\text{small}} &= \frac{\tilde{L}}{2}, \end{aligned} \quad (23)$$

where \tilde{z}_{small} is defined as

$$\tilde{z}_{\text{small}} \equiv \frac{1}{N_{\text{small}}} \sum_i^{N_{\text{small}}} \tilde{z}_i. \quad (24)$$

In Fig. 11 we show for several different ϕ the value of the critical small-chain length N_{small}^* , where the dimensionless aggregation energy barrier to zippering becomes ≤ 1 as a

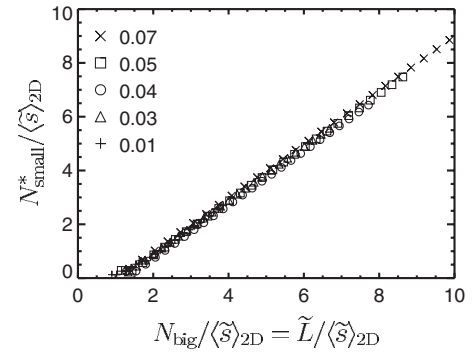


FIG. 12. Scaled critical small-chain length as a function of dimensionless slit thickness scaled by the 2D spacing for five different volume fractions at a dimensionless field strength of $\lambda=50$.

function of \tilde{L} (or N_{big}). For any slit-thickness \tilde{L} and volume fraction ϕ a chain spanning the height of the thin slit can easily zipper with any other chain of length $N_{\text{small}} \leq N_{\text{small}}^*$.

Scaling the lengths in Fig. 11 by the characteristic dimensionless length scale $\langle \tilde{s} \rangle_{2D}$ causes all of the critical small-chain length curves to collapse onto a single master curve as shown in Fig. 12. This is a very important result as it indicates that there is a self-similar behavior of the thin-slit system when the slit thickness is scaled by $\sqrt{\phi}$. Additionally, for our simple model, this result indicates that zippering aggregation begins to occur when $\tilde{L}/\langle \tilde{s} \rangle_{2D} \geq 1.2$. Consequently, if the lowest energy state of the thin-slit system contains clusters with zipped chains, then that state may not be able to be achieved if the energy barriers to zippering are too high. We expect that the dimensionless slit-thickness where the system will depart from 2D behavior should be affected by the energy barriers to zippering and from our model we find that the departure slit thickness will be proportional to $\sqrt{\phi}$ (as predicted by the collapse in Fig. 12).

In Fig. 13 we present the dimensionless spacing between clusters as a function of the dimensionless slit thickness for integer slit thicknesses only. In Fig. 13(a), the departure point of the cluster spacing from 2D behavior depends upon ϕ . Scaling both the dimensionless slit thickness and the dimen-

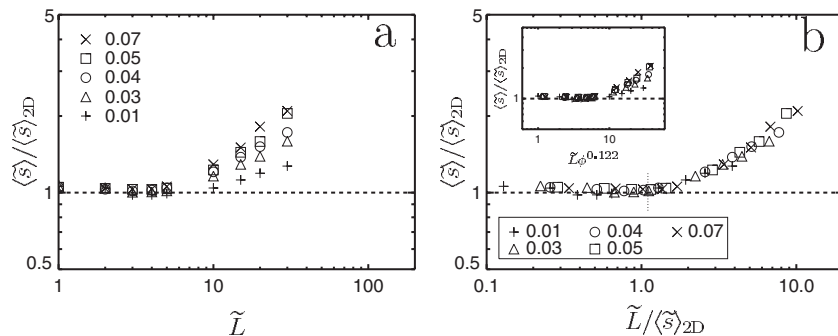


FIG. 13. (a) The average dimensionless spacing between clusters (scaled by the 2D spacing) for five different volume fractions as a function of the dimensionless slit thickness for integer values of \tilde{L} only. (b) The average dimensionless spacing between clusters (scaled by the 2D spacing) as a function of the dimensionless slit thickness (also scaled by the 2D spacing) for five different volume fractions. The horizontal dashed lines are the 2D spacing. The vertical dotted line segment in (b) denotes the point at which our model predicts the dimensionless spacing will deviate from 2D behavior. The inset in (b) shows the average dimensionless spacing between clusters (scaled by the 2D spacing) as a function of the dimensionless slit thickness scaled as predicted by the Gross model [9].

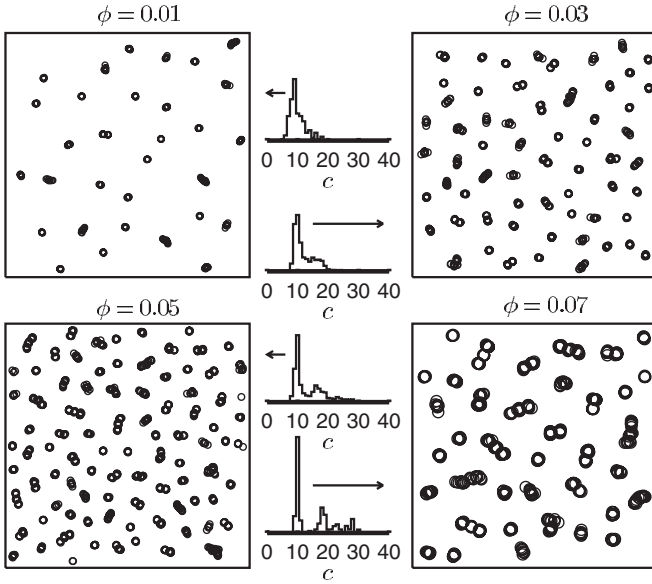


FIG. 14. Top-down views of the thin-slit system for four different volume fractions in a dimensionless slit thickness of 10 at a dimensionless field strength of 50. The cluster-size distributions are shown along the center for volume fractions of 0.01, 0.03, 0.05, and 0.07 (from top to bottom). The fraction of clusters containing zipped chains increases as the volume fraction is increased.

dimensionless spacing between clusters by the 2D spacing ($\langle \tilde{s} \rangle_{2D}$) in Fig. 13(b) we show that the dimensionless slit thickness, where the system departs from 2D behavior is indeed proportional to $\sqrt{\phi}$ and occurs when $\tilde{L}/\langle \tilde{s} \rangle_{2D} \gtrsim 1.2$ [the vertical dotted line segment in Fig. 13(b)]. To further emphasize the importance of this scaling in volume fraction we show in the inset of Fig. 13(b) the collapse of the cluster-spacing curves if we take the ϕ scaling predicted by the Gross model [9]. In Fig. 7 the lowest-energy model shows an abrupt departure from 2D behavior at $\tilde{L} \gtrsim 4$ for $\phi = 0.04$. Based on the lowest-energy model, the departure point from 2D behavior should be proportional to $\phi^{0.122}$, however, it is shown by the poor collapse in the inset of Fig. 13(b) that the departure point does not depend solely upon the lowest energy state but that energy barriers to aggregation are of great importance.

Not only does the model presented here predict the departure from 2D behavior but it also appears in Fig. 13(b) to explain the behavior of the system after the departure as well. Figure 12 shows the self-similar nature of the aggregation of chains in a simple model system. For the thin-slit system, consider a scaled slit thickness of $\tilde{L}/\langle \tilde{s} \rangle_{2D}$ in the range where zippering is energetically feasible (greater than 1.2). At any volume fraction, the scaled lengths of the chains that can zip with a chain of length \tilde{L} are the same. This means that the average cluster size will also scale with $\langle \tilde{s} \rangle_{2D}$ and therefore the spacing between clusters will not have a volume fraction dependence. Thus, all of the scaled spacing curves in Fig. 13(b) collapse for the range of slit-thicknesses studied here.

The volume fraction dependence is further illustrated in Fig. 14, where we show top-down views of the clusters in a dimensionless slit thickness of 10 at four different volume

fractions. The distribution of cluster sizes for each of the four cases is also presented in Fig. 14 showing the increased fraction of zipped clusters as the volume fraction is increased. The left most peak in the cluster distributions is for a cluster size of 10 and the broader peak that appears in the distributions for larger volume fractions is for clusters of zipped chains.

C. Time-scales for zippering

Since zippering is the important mechanism for determining the spacing of clusters we estimate the time scales associated with the zippering of two chains for a fixed volume fraction and slit thickness. If we consider a 2D system of equal numbers of chains of types 1 and 2, then we can analyze the aggregation rate of these two types of chains using ideas from colloid stability theory [22]. Consider a stationary chain of type 2 with chains of type 1 diffusing around it in two dimensions. We will consider the chains to be aligned along the centerline of the thin-slit in the z direction but shifted such that they can zipper, as described previously. This configuration results in the maximum attractive interaction (other than head-to-tail) between two rigid chains confined in a thin slit. If we consider the flux of chains of type 1 in the plane perpendicular to the axes of the chains we can write it as

$$J_1(r) = -D_1 \left[\frac{dn_1}{dr} + n_1 \frac{d\tilde{\Phi}_{12}(r)}{dr} \right], \quad (25)$$

where J_1 is the flux, D_1 is the diffusion coefficient of chains of type 1, n_1 is the area density (number per unit area) of chains of type 1, and $\tilde{\Phi}_{12}(r)$ is the potential energy between a chain of type 1 and a chain of type 2 made dimensionless with $k_B T$. Therefore, the rate of particle flow through a circle of radius r is given by

$$z_1 = -2\pi r D_1 \left[\frac{dn_1}{dr} + n_1 \frac{d\tilde{\Phi}_{12}(r)}{dr} \right], \quad (26)$$

where we consider z_1 to be constant. Defining a new variable

$$y = n_1 e^{\tilde{\Phi}_{12}(r)} \quad (27)$$

we can write the differential of y as

$$dy = \left[\frac{dn_1}{dr} + n_1 \frac{d\tilde{\Phi}_{12}(r)}{dr} \right] e^{\tilde{\Phi}_{12}(r)} dr = \frac{-z_1}{2\pi D_1} e^{\tilde{\Phi}_{12}(r)} \frac{dr}{r}. \quad (28)$$

We define a distance R where the interchain potential [$\tilde{\Phi}_{12}(r)$] goes to zero and the area density of chains of type 1 approaches the average area density for those chains (n_1^{avg}). Using those limits, the integrated form of Eq. (28) is written as

$$n_1(r) = e^{-\tilde{\Phi}_{12}(r)} \left[n_1^{\text{avg}} + \frac{z_1}{2\pi D_1} \int_r^R e^{\tilde{\Phi}_{12}(r)} \frac{dr}{r} \right]. \quad (29)$$

The area density of chains of type 1 goes to zero at contact between the two chains denoted by $r=R_0$. This results in

the rearrangement of Eq. (29) to find the rate of collision between a chain of type 1 and a stationary chain of type 2 to be

$$z_1 = \frac{-2\pi D_1 n_1^{\text{avg}}}{\int_{R_0}^R e^{\tilde{\Phi}_{12}(r)} \frac{dr}{r}}. \quad (30)$$

When the chain of type 2 is also diffusing, the collision rate between chains of type 1 and 2 is given by [22]

$$z_{12} = \frac{-2\pi D_{12} n_1^{\text{avg}}}{\int_{R_0}^R e^{\tilde{\Phi}_{12}(r)} \frac{dr}{r}}, \quad (31)$$

where D_{12} is given by $D_1 + D_2$.

The rate of disappearance of chains of type 1 in this model system due to collisions between chains of type 1 and 2 is therefore given by

$$\frac{dn_1^{\text{avg}}}{dt} = -\alpha n_1^{\text{avg}} n_2^{\text{avg}}, \quad (32)$$

where α is defined as

$$\alpha \equiv \frac{2\pi D_{12}}{\int_{R_0}^R e^{\tilde{\Phi}_{12}(r)} \frac{dr}{r}} \quad (33)$$

and we have multiplied Eq. (31) by the average area density of chains of type 2 (n_2^{avg}), since only a single chain of type 2 was used as a reference chain in solving the diffusive collisions with chains of type 1. If there is an equal area density of chains of type 1 and 2 ($n_1^{\text{avg}} = n_2^{\text{avg}} = n$) then we can simplify the rate of disappearance of chains given in Eq. (32) to be

$$\frac{dn}{dt} = -\frac{\alpha}{2} n^2, \quad (34)$$

where we have dropped the subscripts as we are now considering the area density of all chains (still excluding zipped clusters) and the factor of (1/2) is introduced to avoid counting the same chain twice in the total collision rate (collision of chain i with chain j accounts also for collision of chain j with chain i) [22].

Integrating Eq. (34) gives

$$\frac{n(t)}{n_0} = \left(1 + \frac{t}{t_c}\right)^{-1}, \quad (35)$$

where n_0 is the initial area density of chains [$n(t=0) = n_1^{\text{avg}}(t=0) = n_2^{\text{avg}}(t=0)$] and the time constant t_c is defined as

$$t_c \equiv \frac{2}{\alpha n_0} = \frac{2 \int_{R_0}^R e^{\tilde{\Phi}_{12}(r)} \frac{dr}{r}}{2\pi n_0 (D_1 + D_2)}. \quad (36)$$

In dimensionless form the time constant is given by

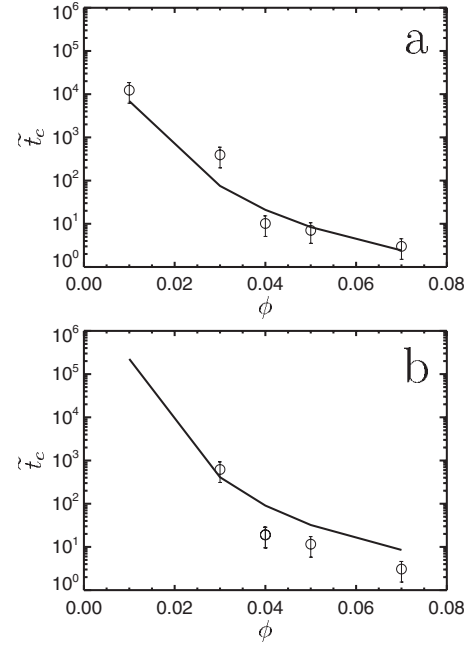


FIG. 15. Mean dimensionless aggregation time, at a dimensionless field strength of 50, as a function of ϕ for (a) a chain of 2 MR colloids to undergo a zipper aggregation with a chain of 5 MR colloids in a dimensionless slit thickness of 5 and (b) a chain of 7 MR colloids to undergo a zipper aggregation with a chain of 10 MR colloids in a dimensionless slit thickness of 10. The solid lines are the theoretical prediction given by Eq. (37) and the circles are the results from BD simulations.

$$\tilde{t}_c = \frac{\langle c \rangle \int_{\tilde{R}_0}^{\tilde{R}} e^{\tilde{\Phi}_{12}(\tilde{r})} \frac{d\tilde{r}}{\tilde{r}}}{6\phi \tilde{L} \left(\frac{1}{N_1} + \frac{1}{N_2} \right)}, \quad (37)$$

where N_1 and N_2 are the number of colloids in a single chain of type 1 and 2, respectively, ϕ is the volume fraction of colloids in the system, and time is again made dimensionless as $\tilde{t} = t(k_B T) / (\zeta d^2)$. Equation (37) assumes Stokes diffusion and that the drag coefficient on a chain is simply proportional to the number of colloids in that chain.

Taking the interchain potentials from the one-dimensional model [$\tilde{\Phi}_{12}(\tilde{r}) = \tilde{U}_c(\tilde{r}) + \beta \tilde{r}$] and choosing the length scale \tilde{R} to be the location of the local minimum in that potential, we can solve Eq. (37) for different chain lengths and volume fractions. In Fig. 15 we show the solution to Eq. (37) (solid line) as a function of ϕ for two different systems, along with the mean times for aggregation from simple BD simulations. The simple BD simulations consisted of eight chains of MR colloids, seven of which spanned the height of the thin slit and the eighth containing three fewer colloids. The chains were started on a hexagonal lattice, oriented in the field direction (z direction), and confined between hard walls inside a simulation box with a dimensionless height equal to the longer chain length. The simulation box had periodic boundary conditions in the other two cartesian directions and the dimensionless lengths of the periodic dimensions were equal

and determined by the volume fraction. The system was simulated using our BD algorithm until the small chain aggregated with one of the larger chains. This procedure was repeated 100 times and the mean time for aggregation was thus calculated.

As shown in Fig. 15, our simple model for the energy between chains as a function of chain length, field strength, and volume fraction is able to qualitatively predict the fact that there are orders of magnitude increases in the timescales for zippering as the volume fraction is decreased. For the case presented in Fig. 15(b) (chains of height 7 and 10), the energy barriers to aggregation are given in Fig. 10(d). For the higher volume fraction cases the chains in the simple simulations zip together much faster than predicted by the model due to the fluctuations of the colloids within the chains [11,23]. When the colloids in a chain are able to fluctuate then the barrier to the zippering aggregation can be reduced and therefore the time for aggregation is also reduced. In Fig. 15(a), the chains are much shorter and the fluctuations of the colloids within the chain are smaller. Since the chains in this case are more rigid, their aggregation behavior is better predicted by our simple model. In both cases however, the timescales for aggregation found in our simple BD simulations show orders of magnitude increases as the volume fraction decreases (and therefore the energy barrier to aggregation increases). In fact, for the case of $\phi=0.01$ we were not able to observe even a single aggregation event for chains of length 7 and 10 in our simple BD simulations when simulating out to dimensionless times of 150 000.

The dimensionless timescale for aggregation from our model for a chain of length 7 to zipper with a chain of length 10 at $\phi=0.03$ and $\lambda=50$ is $\tilde{\tau}_c \sim 410$. The dimensionless energy barrier to aggregation in this case is ~ 4 . For $1 \mu\text{m}$ colloids in water, this translates to a real time of ~ 15.6 min. By comparison, if the short chain length were 8 instead of 7 then the dimensionless energy barrier would be ~ 7.8 and the dimensionless time scale for aggregation would be $\tilde{\tau}_c \sim 13\,783$ or 8.8 h.

IV. DISCUSSION AND SUMMARY

The results presented in this work illuminate several important features of self-assembly of dilute MR fluids confined in extremely thin-slits. Most notably, we have studied the transition from truly 2D behavior to 3D behavior of the structure in the system, manifested in the spacing between clusters. This crossover in the structural properties has not been addressed in previous work. When we extrapolate the models previously developed down to the extremely small slit thicknesses studied in this work we find that a new understanding is needed in order to explain the trends that we observe. We have introduced a simple model for the energy of interaction between chains of MR colloids taking into account the volume fraction of the MR fluid. This model quantitatively addresses the effect of volume fraction upon the energy barriers to aggregation for dilute MR fluids in thin slits. We have used the model to predict the transition point from 2D behavior to 3D behavior in the thin-slit system. In particular, the transition is correlated with the ability of the

chains to begin aggregating laterally into larger columnlike clusters. Our model is able to predict, as a function of volume fraction, at which dimensionless slit thickness this aggregation becomes kinetically feasible. Additionally, in agreement with previous work [2] we find that the 3D behavior of the spacing between clusters follows a power law. Furthermore, our model explains the volume fraction dependence of the self-assembled structures in thin slits when $\tilde{L} \leq 30$. This represents a quantitative analysis of the transition from 2D to 3D behavior for dilute MR fluids self-assembling in the thin-slit system.

We have attempted to use the model for the energy barriers to aggregation in order to predict the timescales for zippering of chains in the thin-slit system. We found qualitative agreement between the predicted time scales and our BD simulations for this aggregation process in that the time scales increase by orders of magnitude as the volume fraction is decreased. During the process of slowly ramping the external field, many short chains will first form with different lengths (Fig. 1) and in order to reach the lowest energy state of zipped clusters, those short chains must aggregate laterally. The time scale of this process will be dominated by the slowest aggregation step which, as we have shown, can be prohibitively long. This point supports the contention that real experimental studies of self-assembly in thin slits can be kinetically trapped in metastable states that only change over extremely long time scales.

As the length scales in microfluidic devices utilizing self-assembled MR fluids shrink, new scalings and models are needed to describe the properties of both the self-assembly and the structures that form in these devices. The previous work on self-assembly of MR fluids in thin slits has not addressed this increasingly important range of phase space where the slits are extremely thin and the MR fluid is dilute. We have shown that the self-assembled structures in extremely thin slits undergo a crossover in their properties from a purely 2D system to the 3D behavior observed previously [2,6,9]. We have shown that this crossover is due to the increased “clustering” of the MR fluid colloids. The crossover is strongly influenced by the energy barriers associated with the zippering aggregation of chains of MR colloids under the extreme confinement induced by the thin slit. It has been postulated that the energetics of the zippering aggregation are important in the self-assembly of MR fluids under confinement in a thin slit but this point has not been quantitatively analyzed in the literature [9,14]. We introduced a model for the energetics of the zippering aggregation and showed how the crossover in behavior from 2D to 3D depends upon the volume fraction of the MR fluid. Using the model for aggregation, we were able to predict the time scales for two chains to aggregate given ϕ , \tilde{L} , and λ . This result leads to the observation that, in certain instances, it is unfeasible for aggregation of chains to occur even though thermodynamics predicts that the aggregated state is the lowest-energy state [9].

Energy barriers appear in many systems in nature and are often important in determining whether a system can reach its lowest energy state. In thin slits the energy barriers to “zippering” have been shown to be quite important in deter-

mining the structure of dilute MR fluids under the application of a uniform magnetic field for dimensionless slit-thicknesses $\tilde{L} < 30$. We note that they are probably also very important for determining the structure of MR fluids in much thicker slits as evidenced by the discrepancy between results presented in the theoretical and experimental literature [1,2,6,7,9,11]. The energy barriers in these thicker slits have not, however, been quantitatively analyzed in the literature due to the much larger complexity involved. The high degree of clustering, including cluster-cluster interactions which

were not investigated here, and the many permutations of possible intra-cluster arrangements of colloids indicate that thicker slits will pose an incredibly challenging problem to be faced in the future.

ACKNOWLEDGMENTS

We gratefully acknowledge the support of NSF NIRT Grant No. CTS-0304128 for this project.

-
- [1] H. Wang, Y. Zhu, C. Boyd, W. Luo, A. Cebers, and R. E. Rosensweig, *Phys. Rev. Lett.* **72**, 1929 (1994).
 - [2] J. Liu, E. M. Lawrence, A. Wu, M. L. Ivey, G. A. Flores, K. Javier, J. Bibette, and J. Richard, *Phys. Rev. Lett.* **74**, 2828 (1995).
 - [3] P. S. Doyle, J. Bibette, A. Bancaud, and J.-L. Viovy, *Science* **295**, 2237 (2002).
 - [4] N. Minc, P. Bokov, K. B. Zeldovich, C. Fütterer, J.-L. Viovy, and K. D. Dorfman, *Electrophoresis* **26**, 362 (2005).
 - [5] J. Liu, T. Mou, Y. Zhu, E. Haddadian, and J. Pousset, *J. Intell. Mater. Syst. Struct.* **7**, 583 (1996).
 - [6] Y. Grasselli, G. Bossis, and E. Lemaire, *J. Phys. II* **4**, 253 (1994).
 - [7] M. Ivey, J. Liu, Y. Zhu, and S. Cutillas, *Phys. Rev. E* **63**, 011403 (2000).
 - [8] L. Zhou, W. Wen, and P. Sheng, *Phys. Rev. Lett.* **81**, 1509 (1998).
 - [9] M. Gross, *Phys. Rev. E* **58**, 6124 (1998).
 - [10] T. C. Halsey and W. Toor, *Phys. Rev. Lett.* **65**, 2820 (1990).
 - [11] J. E. Martin, J. Odinek, and T. C. Halsey, *Phys. Rev. Lett.* **69**, 1524 (1992).
 - [12] M. Fermigier and A. P. Gast, *J. Colloid Interface Sci.* **154**, 522 (1992).
 - [13] T. Ukai and T. Maekawa, *Phys. Rev. E* **69**, 032501 (2004).
 - [14] M. Mohebi, N. Jamasbi, and J. Liu, *Phys. Rev. E* **54**, 5407 (1996).
 - [15] H. Zhang and M. Widom, *Phys. Rev. E* **51**, 2099 (1995).
 - [16] H. C. Öttinger, *Stochastic Processes in Polymeric Fluids: Tools and Examples for Developing Simulation Algorithms* (Springer, Berlin, 1996).
 - [17] R. Haghgoie and P. S. Doyle, *Phys. Rev. E* **70**, 061408 (2004).
 - [18] R. Haghgoie and P. S. Doyle, *Phys. Rev. E* **72**, 011405 (2005).
 - [19] D. Heyes and J. Melrose, *J. Non-Newtonian Fluid Mech.* **46**, 1 (1993).
 - [20] D. Frenkel and B. Smit, *Understanding Molecular Simulation from Algorithms to Applications*, 2nd ed. (MPG Books, Bodmin, 2002).
 - [21] R. Haghgoie and P. S. Doyle, *Europhys. Lett.* **77**, 18002 (2007).
 - [22] P. C. Hiemenz and R. Rajagopalan, *Principles of Colloid and Surface Chemistry* (Marcel Dekker, New York, 1997).
 - [23] E. M. Furst and A. P. Gast, *Phys. Rev. E* **62**, 6916 (2000).